

Numerical simulation of hybrid rocket engine flowfields

D. Bianchi, A. Urbano, B. Betti and F. Nasuti
Sapienza University of Rome
Department of Mechanical and Aerospace Engineering
Via Eudossiana 18, I-00184 Rome, Italy

Abstract

Numerical simulations of the flow in a GOX/HTPB hybrid rocket engine are carried out with a Reynolds averaged Navier-Stokes solver including detailed gas surface interaction mass and energy balances. Global mechanisms are considered for the gas-phase chemistry. Results show the role of the gas-phase chemistry modeling and surface boundary condition modeling on the solution. The effect of chemical species distribution in the wall region on a nozzle carbon-carbon wall is finally discussed.

1. Introduction

The intrinsic properties of hybrid propellant rockets in terms of performance, simplicity, safety, reliability, low development cost, reduced environmental pollution, and flexibility, make them as one of the envisaged future generation propulsion systems [1]. Nevertheless, the hybrid rocket engine development has not achieved the same level of maturity as solid and liquid traditional systems. Therefore, as the new international attention to hybrid propulsion points out, the hybrid system design needs a better understanding of the physico-chemical phenomena that control the combustion process and of the fluid dynamics inside the motor [1, 2, 3]. The knowledge of the complex interactions among fluid dynamics, solid fuel pyrolysis, oxidizer atomization and vaporization, mixing and combustion in the gas phase, particulate formation, and radiative characteristics of the gas and the flame can only be improved by combined experimental and numerical research activities. Similar considerations can be made regarding the ablation process of the nozzle thermal protection system (TPS). The numerical study of the flow in the combustion chamber and in the nozzle of a hybrid propellant rocket requires the ability to describe adequately the interaction between the reacting flow and the solid surface through suitable gas-surface interaction (GSI) modeling.

In a classical hybrid propellant rocket, the liquid or gaseous oxidizer injected into the ports of solid fuel grain reacts in the combustion chamber with the pyrolysis gas, which is produced on the surface and diffuses into the boundary layer, forming a turbulent diffusion flame. The convective and radiative heat flux from the flame, in turn, provides the energy needed for the pyrolysis process of solid fuel. It is evident that the fuel regression rate is governed by the interaction between these different processes. The solid fuel in a hybrid rocket regresses slowly making in fact necessary to use a large fuel surface exposed to hot gas to get the mass flow rate required by the motor design. The solid fuel regression rate and its dependence on various operating conditions is therefore of basic importance in the design and development of hybrid rockets. Classical studies on hybrid propulsion are based on simplified models of the boundary layer to derive the heat flux to the surface of the solid fuel and, therefore, its regression rate [4]. However, this simplified analysis can not take into account many of the complex chemical and physical interactions between the various processes, such as the effect of changes in operating conditions, chamber pressure, radiation and finite-rate chemistry, making necessary the development of more advanced models based on computational fluid dynamics (CFD) to improve prediction and analysis capabilities for such propulsion systems. A common approach is therefore that of solving the Reynolds averaged Navier-Stokes (RANS) equations, with suitable turbulence closure models. In particular, there is an interest in obtaining steady-state solutions by solving RANS equations, as justified by the fact that chemical and fluid-dynamic time scales are much faster than the regression rate time scale. Therefore, a valid approach to study the hybrid rocket internal ballistics can be that of simulating the flow at different times thus considering different chamber geometries [5]. However, in addition to the equations of motion, the various physical phenomena and chemical characteristics of these propulsion systems have to be suitably modeled: the coupling between the gas and solid phase based on mass and energy balances, the fuel surface pyrolysis and regression rate, the finite-rate chemistry to describe the combustion process, and the turbulent diffusion of oxidizing species and of the pyrolysis gas.

The objective of this study, which is carried out within the framework of an Italian project [6], is the simulation of the flow inside the combustion chamber and nozzle of a hybrid rocket. In the present study, a simplified kinetic

model is adopted, i.e. a comprehensive combustion model, based on a small number of reaction steps [7]. In fact, a detailed model of chemical kinetics is very complicated and, in this case, could involve more than 50 chemical species and hundreds of elementary reaction steps [5]. A simplified kinetic model reduces the computing time by reducing the number of species involved in the overall reaction and is therefore the most efficient way to achieve the goal of a complete modeling of physical-chemical processes within a hybrid rocket and therefore to validate the simulation model. Regarding the process of solid fuel pyrolysis, it can be described by semi-empirical models (such as those proposed in [8, 9]) in which the rate of pyrolysis is expressed through an Arrhenius type relationship where the unknowns are the solid fuel surface temperature and regression rate. Suitable boundary conditions have to be introduced to describe the solid-gas coupling which is necessary to obtain the flow field solution. This boundary condition on the solid fuel surface requires mass and energy balances, which, together with pyrolysis and gas-phase combustion models, yield a coupled gas-surface solution. The surface energy balance involves different contributions to wall heat flux: the convective heat flux related to temperature gradient, the heat flux related to diffusive gradients of concentration, the possible radiative heat flux, the conduction heat flux in the solid phase, and the pyrolysis heat flux due to mass injection in the flow field. A similar mass balance can be defined for each chemical species considering the diffusive flux, the convective flux due to mass injection, and the source term due to thermal decomposition during the pyrolysis process. The model for the boundary condition developed in [10, 11] for the ablative thermal protection is also based on surface mass and energy balances and this model is extended here to the case of solid fuel pyrolysis. Finally a model has to be introduced to describe the heat conduction within the solid fuel. Similarly to what done for the analysis of ablative thermal protection systems, the assumption of steady-state thermal field within the fuel can be made, which is considered appropriate for the hybrid rocket conditions [5].

The numerical simulations are carried out by solving Reynolds averaged Navier-Stokes equations for single-phase multicomponent reacting flows, including the required sub-models in order to describe: homogeneous combustion in the gas phase, fluid-surface interaction in the combustion chamber (solid fuel pyrolysis model) and fluid-surface interaction in the nozzle (material thermochemical ablation model). The in-house code used for the simulations has been validated for re-entry flows [12], whereas the same gas-surface interaction model has been used for the study of hybrid rocket nozzle flowfields and thermal protection system behavior [13]. The results obtained by preliminary simulations carried out with the present approach are presented and discussed. Simulations are based on a reference test case of a hybrid rocket engine with propellants GOX (Gaseous oxygen) and HTPB (Hydroxyl-Terminated Poly-Butadiene) taken from the literature [5].

2. Theoretical and numerical model

The study of hybrid rocket engine flowfields requires a suitable modeling of both gas-surface interaction and gas phase reactions. In the present study the modeling of gas-surface interaction already developed and validated for ablating surface is extended to the case of pyrolysis of hybrid rocket engine fuel. The modeling of gas/surface interactions has been the subject of considerable interest recently, because the coupling that occurs has been shown to have a dramatic effect on the net heating level induced by the gas and on the response of the surface. In particular, a detailed finite-rate gas/surface reaction model is coupled with a three-dimensional chemically-reacting fluid dynamics (CFD) code. The boundary condition with general non-equilibrium finite-rate chemistry for gas/surface interaction is used to predict the mass injection rate thus providing full thermal chemistry coupling in the CFD simulation in case of thermochemical erosion of carbon-carbon TPS and HTPB fuel pyrolysis.

2.1 Gas/surface interface

If it is assumed that no material is being removed in a condensed phase (solid or liquid), then the general conservation laws at the gas-solid interface for a non-decomposing material can be written as [14, 15]:

$$\dot{m}_w = \rho v = \rho_s \dot{s} \quad (\text{Mass balance}) \quad (1)$$

where \dot{m}_w is overall mass flow rate injected at wall, ρ and v are density and the normal-to-wall velocity in the gas phase due to wall consumption products injection, and finally ρ_s while \dot{s} are the solid material density and regression rate, respectively;

$$\rho D_{im} \frac{\partial y_i}{\partial \eta} + \dot{\omega}_i = \rho v y_i \quad i = 1, N \quad (\text{Species mass balance}) \quad (2)$$

where D_{im} is the species-to-mixture diffusion coefficient, η the normal-to-wall outward coordinate (directed from wall to gas), y_i the gas phase mass fraction, N the number of species, and $\dot{\omega}_i$ is the rate of production of gas-phase species i

at the nozzle surface due to heterogeneous reactions;

$$k \frac{\partial T}{\partial \eta} + \sum_{i=1}^N h_i \rho D_{im} \frac{\partial y_i}{\partial \eta} + \dot{q}_{rad,in} + \dot{m}_w h_s = \dot{m}_w h + \dot{q}_{rad,out} + \dot{q}_{cond}^{ss} \quad (\text{Energy balance}) \quad (3)$$

where h is the enthalpy of the gas mixture, h_i the enthalpy of the single gas species, h_s the enthalpy of the solid, k the gas conductivity, T the gas temperature, $\dot{q}_{rad,in}$ and $\dot{q}_{rad,out}$ radiation heat flux entering and exiting the wall, respectively, and \dot{q}_{cond}^{ss} the conduction heat flux inside the wall. The superscript $()^{ss}$ indicates that the steady state assumption is made for solid heat flux conduction. The conduction term, at steady-state, depends on the material regression rate \dot{s} and on the material density and enthalpy through a closed form [16]. In fact, if the heat conduction process inside the wall is treated as one-dimensional, when the steady-state condition of a planar surface is considered, the closed solution of the in-depth energy balance can be achieved from its integration between the hot (front) surface and the cold (back) surface of the material. Therefore, the steady-state solid conduction term reads:

$$\dot{q}_{cond}^{ss} = \dot{m}_w (h_s - h_{s_0}) \quad (4)$$

where h_s and h_{s_0} represent the enthalpy of the solid material at the wall temperature and at the initial temperature, respectively.

The energy balance expression can be recasted using Eq. (2) emphasizing the contributions due to convection from the gas, conduction into the wall, radiation and chemical reactions, as:

$$\underbrace{k \frac{\partial T}{\partial \eta}}_{\text{convective}} = \underbrace{\sum_{i=1}^N \dot{\omega}_i h_i - \dot{m}_w h_s}_{\text{chemical}} + \underbrace{\dot{q}_{rad,in} - \dot{q}_{rad,out}}_{\text{radiation}} + \underbrace{\dot{q}_{cond}^{ss}}_{\text{conduction}} \quad (5)$$

Note that the term $\dot{m}_w h_s$ is the energy flux entering the surface due to surface consumption.

The rate of production of gas-phase species i at the nozzle surface, $\dot{\omega}_i$ appearing in Eqs. (2) and (5), has to be estimated on the basis of solid fuel or nozzle material and combustion gas chemical composition. Let us first discuss the case of nozzle material. The rocket-nozzle material considered in the present study is graphite, which is one of the most widely used nozzle materials. The heterogeneous gas-surface chemical reactions are described by a semi-global heterogeneous reaction mechanism for graphite oxidation consisting of five reactions [17, 18]. A subset of this reaction mechanism, excluding erosion contributions from species O and O₂ whose concentration is negligible small in solid rocket combustion products, has been recently validated for graphite nozzle erosion in solid rocket motors [11, 19, 20].

Table 1: Heterogeneous rate constants and reaction order of graphite with H₂O, CO₂, OH, O, and O₂ [17, 18]

Surface reaction	j	A_j	E_j , kJ/mol	b_j	n_j
$C_s + H_2O \rightarrow CO + H_2$	1	4.8×10^5	288	0.0	0.5
$C_s + CO_2 \rightarrow 2CO$	2	9.0×10^3	285	0.0	0.5
$C_s + OH \rightarrow CO + H$	3	3.61×10^2	0.0	-0.5	1.0
$C_s + O \rightarrow CO$	4	6.655×10^2	0.0	-0.5	1.0
	5	2.4×10^3	125.6	0.0	-
	6	2.13×10^1	-17.17	0.0	-
$C_s + \frac{1}{2}O_2 \rightarrow CO$	7	5.35×10^{-1}	63.64	0.0	-
	8	1.81×10^7	406.1	0.0	-

With this mechanism, the contribution to erosion due to the i -th species can be expressed as (in kg/m² · s):

$$\dot{m}_i = k_j p_i^{n_j} \quad \text{for species } i = H_2O, CO_2, OH, \text{ and } O \quad (6)$$

where p_i is the partial pressure (in atm) of the oxidizing species i , n_j is the overall order of the heterogeneous j th reaction, and k_j is the specific rate constant of j th reaction, which can be expressed by an Arrhenius type expression:

$$k_j = A_j T^{b_j} \exp(-E_j/RT) \quad (7)$$

where T is the wall temperature (in K) and A_j , b_j , and E_j are the pre-exponential factor, the temperature exponent, and the activation energy for the j th reaction, respectively. The reaction order n_j and the kinetic parameters of Eq. (7)

for the reactions of graphite with H₂O, CO₂, OH, and O are taken from Refs. [17, 18] and are listed in Table 1, where are reported the value to be inserted for k_1 , k_2 , k_3 , and k_4 which are respectively expressed according to Eq. (7). The surface reaction rate with molecular oxygen cannot be properly expressed by a linear Arrhenius expression as that of Eq. (6), and therefore the kinetic expression by Nagle and Strickland-Constable [21] is used:

$$\dot{m}_{O_2} = \frac{k_5 p_{O_2} Y}{1 + k_6 Y} + k_7 p_{O_2} (1 - Y) \quad \text{where } Y = \left(1 + \frac{k_8}{k_7 p_{O_2}}\right)^{-1} \quad (8)$$

The kinetic parameters of Eq. (8) for the reaction of graphite with O₂, with k_5 , k_6 , k_7 , and k_8 expressed according to Eq. (7), are taken from Refs. [17, 18] and are also listed in Table 1.

The total erosion rate of carbon due to the surface heterogeneous reactions is finally expressed as:

$$\dot{m}_w = \dot{m}_{H_2O} + \dot{m}_{CO_2} + \dot{m}_{OH} + \dot{m}_O + \dot{m}_{O_2} = \rho_s \dot{s} \quad (9)$$

The rate of production/consumption of the generic gas-phase species i at the nozzle surface, $\dot{\omega}_i$ in Eq. (2), can be easily derived from the rate of erosion of carbon by the generic oxidizing species, Eqs. (6) and (8), and the mass balance available once the species molecular weights and the stoichiometry of the surface reactions are known (Table 1). The surface mass and energy balances are intimately coupled, and therefore they must be solved jointly: with the wall pressure coming from the flow-field (assuming zero-pressure gradient at wall) and with the wall temperature computed from the surface energy balance, Eq. (3), the chemical composition at the nozzle wall and the net erosion rate can be obtained from Eqs. (2), (6), (8), and (9) using an iterative algorithm to satisfy the energy balance, Eq. (3).

The chemical source terms in Eq. (2), $\dot{\omega}_i$, are defined as:

$$\dot{\omega}_{CO} = (M_{CO}/M_C) (\dot{m}_{H_2O} + 2\dot{m}_{CO_2} + \dot{m}_{OH} + \dot{m}_O + \dot{m}_{O_2}) \quad (10)$$

$$\dot{\omega}_{CO_2} = -\dot{m}_{CO_2} (M_{CO_2}/M_C) \quad (11)$$

$$\dot{\omega}_{H_2O} = -\dot{m}_{H_2O} (M_{H_2O}/M_C) \quad (12)$$

$$\dot{\omega}_{OH} = -\dot{m}_{OH} (M_{OH}/M_C) \quad (13)$$

$$\dot{\omega}_{H_2} = \dot{m}_{H_2O} (M_{H_2}/M_C) \quad (14)$$

$$\dot{\omega}_H = \dot{m}_{OH} (M_H/M_C) \quad (15)$$

$$\dot{\omega}_i = 0 \quad \text{for the remaining gaseous species} \quad (16)$$

where M indicates the molar mass of a given species. With the wall pressure coming from the flow-field (assuming zero-pressure gradient at wall) and with the wall temperature computed from the surface energy balance Eq. (5), the chemical composition at the nozzle wall and the net erosion rate can be obtained from Eq. (2), (6), (9), and (10–16).

For the case of solid fuel consumption a simpler model is adopted. In fact, according to [5], a single Arrhenius type equation is used to model \dot{m}_w . In particular, the rate of pyrolysis is obtained as:

$$\dot{m}_w = A_9 \exp(-E_9/RT) \quad (17)$$

where coefficients are taken as reported in Table 2, according to Arisawa and Brill [9]. The corresponding chemical

Table 2: Heterogeneous rate constants for HTPB [5]

Surface reaction	j	A_j	E_j , kJ/mol
HTPB _s → C ₄ H ₆	9	2.208 x 10 ³	288

source terms in Eq. (2), $\dot{\omega}_i$, are defined as:

$$\dot{\omega}_{C_4H_6} = \dot{m}_w \quad (18)$$

$$\dot{\omega}_i = 0 \quad \text{for the remaining gaseous species} \quad (19)$$

2.2 Gas phase reactions

Finite-rate gas surface reactions, are modeled by global reaction mechanisms, because detailed chemical kinetics mechanism would include many species and would be from one side computational heavy and from the other side beyond the

scope of the present study, whose aim is to focus on gas-surface interaction. Therefore, according to [5] the first global mechanism considered is a global combustion model, involving two reaction steps. The first reaction is between C_4H_6 , which is the representative HTPB pyrolysis product yield from the gas-surface interaction mechanism, and molecular oxygen. The second reaction accounts for the formation and consumption of CO.



The resulting rates of production and destruction of species are:

$$\dot{w}_{C_4H_6} = -M_{C_4H_6}k_{f_1}[C_4H_6][O_2] \quad (22)$$

$$\dot{w}_{O_2} = M_{O_2}[-3.5k_{f_1}[C_4H_6][O_2] - 0.5(k_{f_2}[CO][O_2]^{0.5} - k_{b_2}[CO_2])] \quad (23)$$

$$\dot{w}_{CO} = M_{CO}\{4k_{f_1}[C_4H_6][O_2] - (k_{f_2}[CO][O_2]^{0.5} - k_{b_2}[CO_2])\} \quad (24)$$

$$\dot{w}_{H_2O} = 3M_{H_2O}k_{f_1}[C_4H_6][O_2] \quad (25)$$

$$\dot{w}_{CO_2} = M_{CO_2}(k_{f_2}[CO][O_2]^{0.5} - k_{b_2}[CO_2]) \quad (26)$$

The forward and backward reaction rates k_f and k_b for the two reactions are expressed as Arrhenius functions, and the values of the constants used in this study are tabulated in Table 3.

Table 3: Reaction rates constants for reactions (20) and (21)

Reaction rate	A	E/R, K
k_{f_1}	1.3496×10^{10}	15108
k_{f_2}	2.2387×10^{12}	20143
k_{b_2}	5.0000×10^{10}	20143

3. Results and Discussion

3.1 Nozzle thermochemical erosion

A first series of results has been obtained analyzing the behavior of graphite nozzle TPS under the action of combustion products of GOX/HTPB hybrid rocket engine. The baseline nozzle geometry employed is the one used in the BATES (Ballistic Test and Evaluation System) experimental solid rocket motor, which has been rebuilt on the basis of the main geometric parameters reported in [22]. The BATES motor as well as the CFD pressure field and nozzle grid are shown in Fig. 1. The nozzle throat radius is 2.54 cm, with a 45° conical convergent section and a 15° conical divergent section. As shown in Fig. 1, the convergent section has been reproduced using a parabolic curve, which becomes parallel to

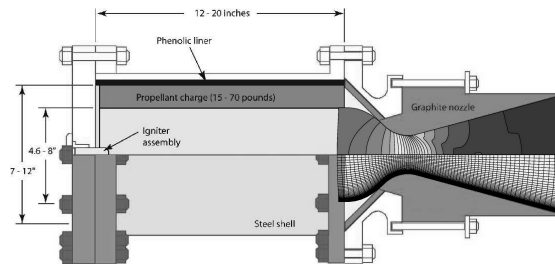


Figure 1: BATES motor configuration [22] with CFD pressure field and nozzle grid

the nozzle axis at the inlet section so that an axial inlet velocity profile can be assigned. Since the length of the wall is important, because it affects the boundary-layer thickness and hence the heat and mass transfer rate, the total wall length of the parabolic curve is equal to that of the 45° cone. These assumptions have been successfully validated in [11] for the study of nozzle throat erosion as a function of propellant composition using the BATES motor configuration. In accordance with the BATES nozzle erosion test, the nozzle material is bulk graphite ($\rho_s = 1.83 \text{ g/cm}^3$). The hot exhaust gas flowing in the nozzle consists of the equilibrium combustion products for HTPB and GOX. Chamber conditions

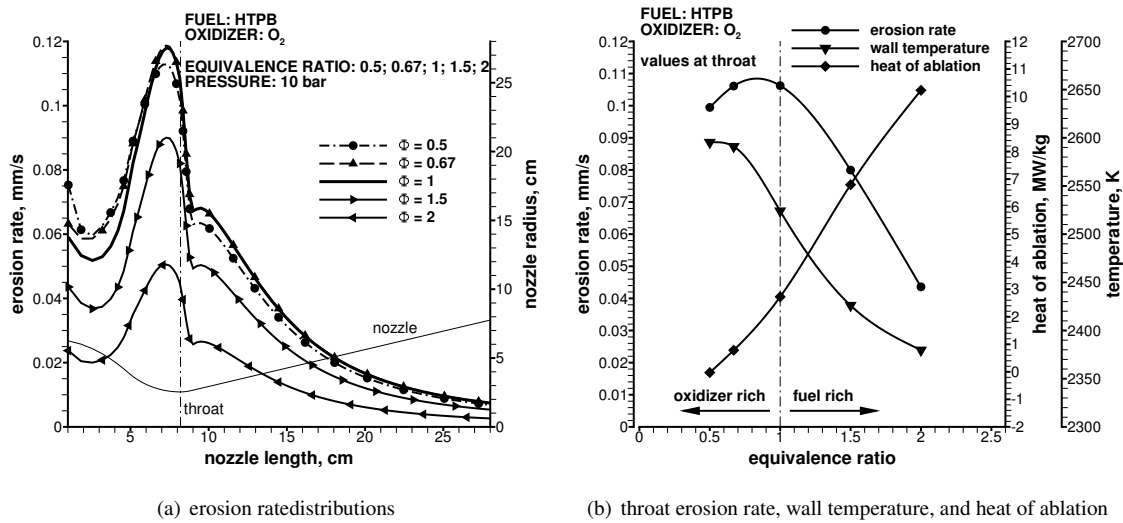


Figure 2: Nozzle erosion response for HTPB and oxygen at varying equivalence ratios

have been obtained for the analysis of TPS behavior by a chemical equilibrium code [23] at a pressure of 10 bar and for different values of the equivalence ratio, ϕ . The chamber pressure level has been chosen to represent the value used in the experimental test campaign which is going to be performed in the framework of the project “Development and integration of the Italian scientific expertise for the progress of hybrid rocket engines” [6], supported by the Italian Ministry of Education, University and Research (MIUR). Ten species (CO , CO_2 , H_2 , H_2O , N_2 , OH , H , NO , O , and O_2) have been considered for each equilibrium simulation as they constitute, for each case, more than 99.9% of the total combustion gas mass. A large part of the exhaust gas mass ($\sim 70\%$) is constituted by oxidizing species. The computational domain is subdivided into 70×80 grid points in the axial and radial directions, respectively. The meshes are clustered towards the wall such to ensure a value of y^+ less than 1.0 at the wall-adjacent cell all along the nozzle length to accurately describe the boundary layer. All the computations presented here are at the steady-state condition obtained by iterating in time until residuals drop by five orders of magnitude. A finer numerical grid, made of 140×160 grid points, has been considered giving erosion rates in the throat section deviating less than 2% from the ones obtained using the standard grid, which has therefore been considered sufficiently refined for the present study.

As a peculiar characteristic of hybrid rocket engines is the intrinsic shifting of the O/F ratio during both steady-state operation and throttling, different values of O/F and this of the equivalence ratio are considered. Typically, shifts in mixture ratio during burn can involve both fuel-rich and oxidizer-rich conditions.

The effect of O/F shifts on the nozzle erosion rate has been analyzed for a wide range of mixture ratio. The starting point is given by the results at stoichiometric conditions. Subsequently, for fuel-rich conditions, the fuel is increased by 50 and by 100% with respect to its stoichiometric value. For oxidizer-rich conditions, the same increases are applied to the oxidizer. This leads to equivalence ratios (defined here as the ratio of the fuel-to-oxidizer ratio to the stoichiometric fuel-to-oxidizer ratio) of 1.5 and 2.0 for fuel-rich conditions, and 0.67 and 0.5 for oxidizer-rich conditions. Typically, the flame temperature shows a maximum for the stoichiometric condition, and tends to equally decrease for fuel- or oxidizer-rich mixtures. Radical species such as O and OH , which are shown to react at high rates with graphite, usually peak close to the stoichiometric condition, due to the higher flame temperature which favors their production. The dominant oxidizing species H_2O , instead, tends to increase for mildly fuel-rich conditions ($\Phi \approx 1.5$) due to the increasing hydrogen content in the mixture. Differently, O_2 concentration is rising continuously as the mixture ratio becomes increasingly oxidizer-rich. Figure 2 shows the nozzle erosion response for HTPB and oxygen at varying equivalence ratios. Interestingly, the erosion rate is mildly affected by the mixture ratio for oxidizer-rich conditions, while it is strongly reduced for fuel-rich conditions. This is due to the fact that, while flame temperature is reduced when off-stoichiometric mixture are considered, molecular oxygen presence in the combustion gases is greatly increased for oxidizer-rich mixtures thus leading to a heat release by the corresponding graphite oxidizing reaction which in turn increases the wall temperature and the overall reaction rate. When oxygen is used as oxidizer, in fact, for $\Phi = 0.5$, the erosion rate is only reduced by 6% if compared to stoichiometric conditions but the molecular oxygen contribution to total erosion increases from 8.4% to 27%. The wall temperature at the throat is 2595 K for $\Phi = 0.5$, which is 70 K higher than the wall temperature at stoichiometric conditions even if the flame temperature is 280 K lower. Despite a significant reduction in flame temperature, the wall temperature is higher due to the heat release of

the oxidizing reactions at the surface. As clearly indicated in Fig. 2(b), in fact, the heat of ablation is reducing as Φ is reduced and for some conditions it can also reach negative values, meaning that the surface reactions are releasing heat. Similar trends can be obtained for all the other combinations of fuels and oxidizers. However, due to the high content of water vapor in the exhaust gases, the heat of ablation is always positive when hydrogen peroxide is used as oxidizer.

3.2 Fuel pyrolysis and combustion

The implementation of the boundary conditions needed to simulate the flowfield in hybrid rocket engine combustion chambers has been successfully made leading to preliminary results. These preliminary results have been obtained on a basic planar channel test case. The fuel is HTPB and the oxidizer is gaseous oxygen. The only considered pyrolysis gas is C_4H_6 which is injected from the upper wall in a gaseous oxygen mass flow. Gaseous oxygen is injected at a total temperature of 300 K and a total pressure of 30.8 bar. Channel height is 2 mm, whereas its length, through which HTPB is injected is 1 cm. Dimensions and flow conditions are inspired to the work of [5].

A first set of computations has been carried out considering a constant wall temperature and therefore a constant blowing mass flow rate. If wall temperature is enforced, meaning that the energy balance which determines the wall temperature is not used in the calculations, according to Eq. (17) also the mass flow rate per unit area of injected fuel is constant. Different temperatures have been considered between 800 and 900 K with the aim of understanding the blowing influence over the diffusive flame position and temperature. The one step kinetic mechanism given by Eq. (20) has been considered for this first parametric set. Results are shown in Fig. 3 where profiles of temperature, reactants mass fractions and products mass fractions are compared in a section at the end of the domain ($x/D = 2.5$). It is interesting to note that all the fuel is burned in a short distance from the wall. Nevertheless, combustion reactions peak outside of the boundary layer. Increasing the wall temperature, according to Eq. (17), the blowing mass flow rate increases and this influences the diffuse flame. As a consequence the maximum temperature increases and the flame stabilizes farther from the wall.

In the same figure are also reported the results obtained if the energy balance equation Eq. (3) is considered to deduce the wall temperature. A formation enthalpy of $h_{s0} = -579.07 \cdot 10^3$ J/kg has been considered for the HTPB. For the considered section ($x/D = 2.5$), results obtained applying the energy balance are very similar to the 850 K isothermal wall case. Actually, the wall temperature computed from the energy balance varies along the channel axis and is shown in Fig. 4(a) (red line): the wall temperature has a peak at the channel entrance because of the thermal boundary layer formation and then decreases and assumes values between 800 and 900 K, in accordance with literature [5]. The blowing mass flow rate can be computed from the wall temperature and Eq. (17) and the regression rate follows according to Eq.(1). The regression rate has been computed considering a HTPB density of $\rho_s = 930$ kg/m³ and is shown in Fig. 4(b) (blue line). After the initial peak due to the boundary layer formation, the regression rate tends towards values between 0.5 and 1 mm/s which are of the order of magnitude that can be expected for the considered configuration.

Finally, the two-steps mechanism given by equation Eqs. (20) and (21) and the energy balance equation for the boundary conditions have been considered for the same test case. Temperature and reactant species fields, considering the one or two-steps mechanisms, are compared in Figs. 5(a), 5(b) and 5(c). The role of the mechanism is important as shown by the temperature field: the maximum temperature reached is around 3400 K for the one step mechanism and 4700 K for the two-steps one. In fact, the second reaction behaves as exothermic and therefore increases the gas product temperature as shown in Fig. 5(a). The energy balance gives a higher wall temperature and, as a consequence, a high regression rate as shown in Fig. 4. Consequently this affects both the position of the flame (the maximum temperature moves towards the channel axis) and the reactants fields. More precisely, for the two-steps mechanism case, higher percentages of C_4H_6 can be found near the wall as shown in Fig. 5(c).

Results agree well with those of [5], meaning that the correct implementation has been made. From this starting point the activity can be carried on to analyze the effect of combustion on the radial gradients and thus on the nozzle erosion.

Acknowledgments

This study is supported by the Italian Ministry of University and Scientific Research in the framework of the Progetto di Ricerca di Interesse Nazionale (PRIN) project: Numerical models for the analysis of ablation and combustion in hybrid propellant rockets.

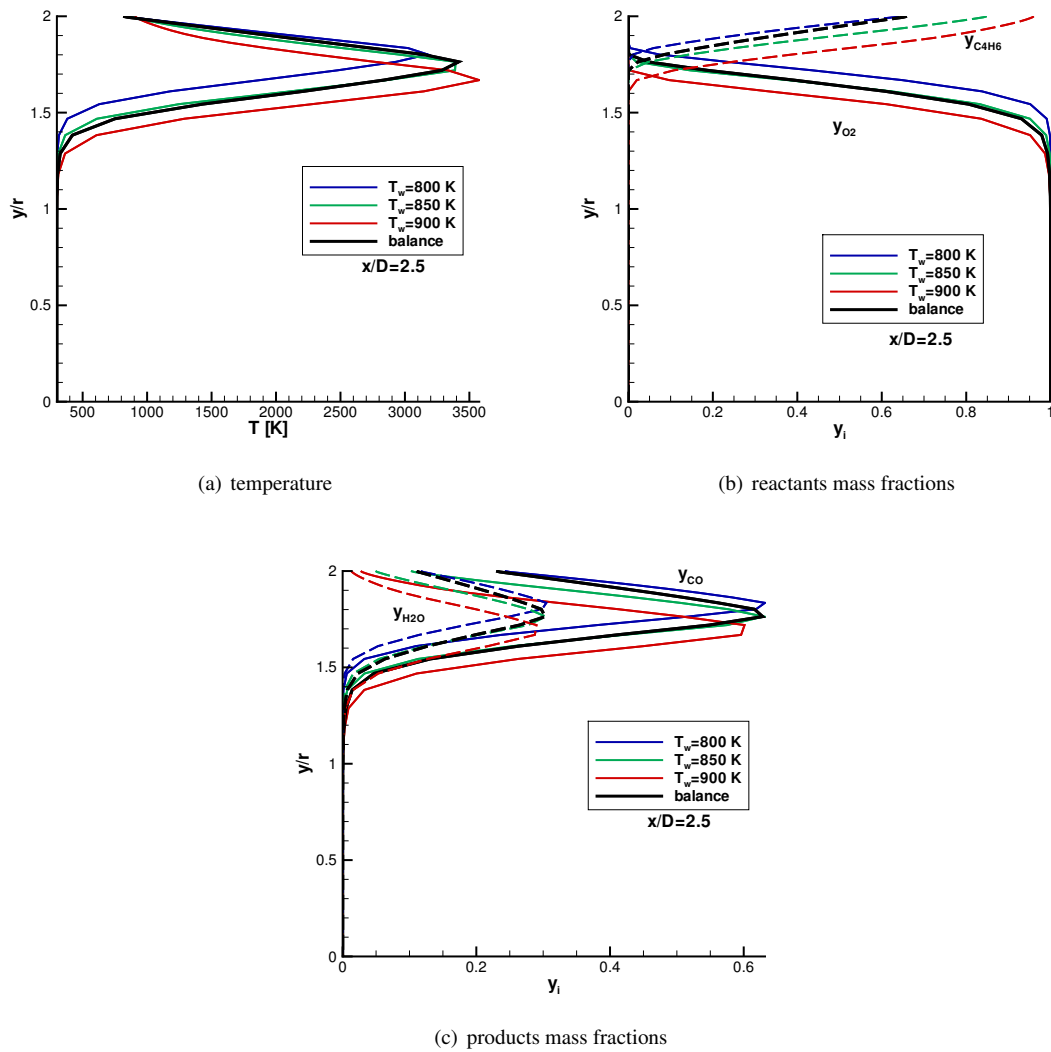


Figure 3: Temperature and species mass fractions profiles in $x/D = 2.5$. Comparison between isothermal wall boundary condition (colors) and energy balance boundary condition (black).

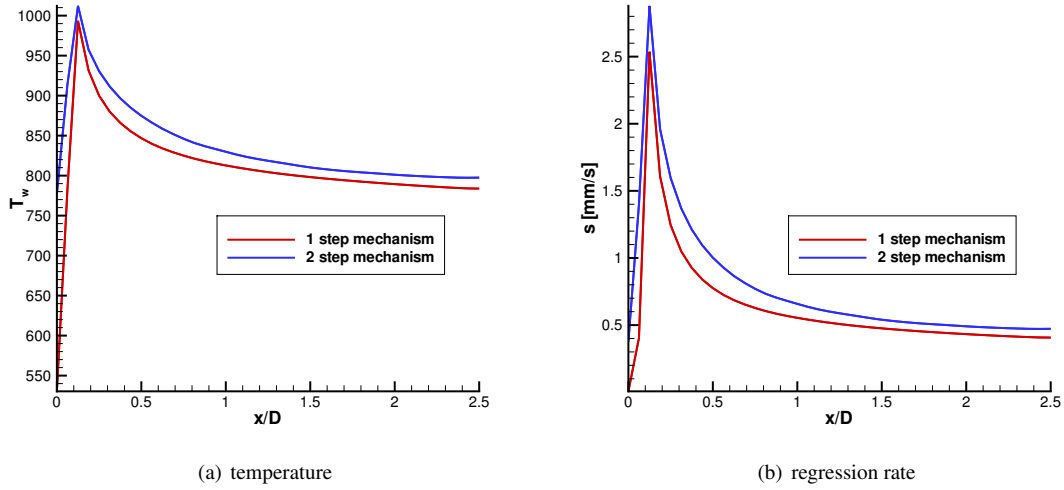


Figure 4: Wall temperature and regression rate computed considering 1 or 2 step kinetic mechanisms

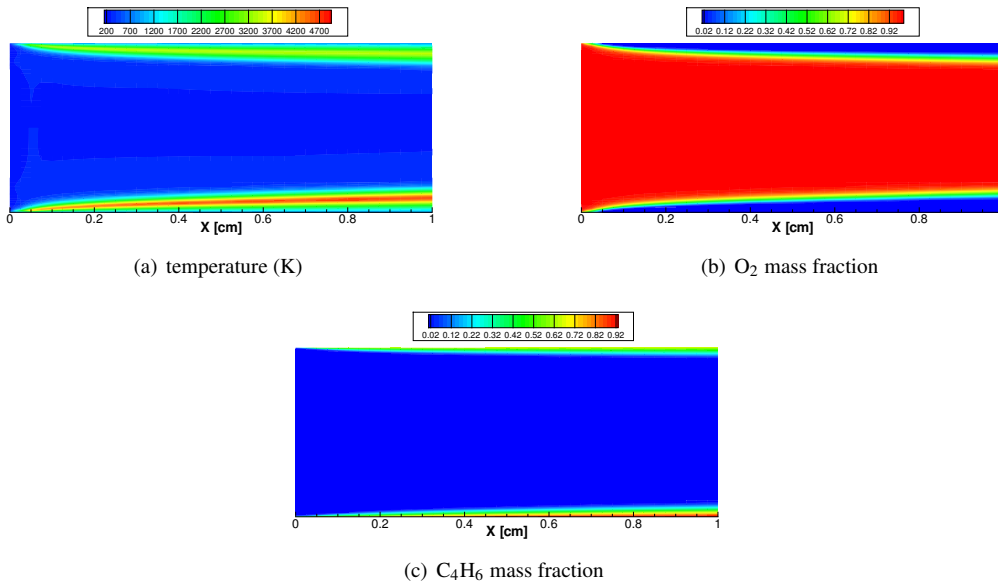


Figure 5: Temperature and species mass fraction fields. Comparison between one-step (up) and two-steps (down) mechanism

References

- [1] Kuo, K. K. and Houim, R. W., 2011. Theoretical Modeling and Numerical Simulation Challenges of Combustion Processes of Hybrid Rockets. AIAA Paper 2011-5608.
- [2] De Luca, L. T., Galfetti, L., Maggi, F., and Colombo, G., 2009. Advances in Hybrid Rocket Propulsion. 3rd European Conference for Aero-Space Sciences, Versailles, France, 6-9 July 2009.
- [3] Carmicino, C. and Russo Sorge, A., 2005. Role of Injection in Hybrid Rockets Regression Rate Behavior. *Journal of Propulsion and Power*. 21(3):606–612.
- [4] Kuo, K. K. and Chiaverini, M., 2007. Challenges of Hybrid Rocket Propulsion in the 21st Century. *Fundamentals of Hybrid Rocket Combustion and Propulsion*, edited by K. Kuo and M. Chiaverini. *Progress in Astronautics and Aeronautics* 218:593–638.
- [5] Sankaran, V., 2007. Computational Fluid Dynamics Modeling of Hybrid Rocket Flowfields, *Fundamental of Hybrid Rocket Combustion and Propulsion*, edited by K. Kuo and M. Chiaverini. *Progress in Astronautics and Aeronautics* 218:323–349.
- [6] Galfetti, L., Nasuti, F., Pastrone, D., and Russo, A., 2012. An Italian Network to Improve Hybrid Rocket Performance: the Strategy, the Program, the Results. Tech. rep., 2012, IAC-12-C4.2.9, 63rd International Astronautical Congress, Naples, Italy, 1-5 October, 2012.
- [7] Westbrook, C. and Dryer, F., 1981. Simplified reaction mechanism for the oxidation of hydrocarbon fuels in flames. *Combustion science and technology*. 27:31–43.
- [8] Cohen, N., Fleming, R., and Derr, R., 1974. Role of binders in solid propellant combustion. *AIAA Journal*, 12:212–218.
- [9] Arisawa, H. and Brill, T. B., 1996. Flash pyrolysis of Hydroxyl Terminated Poly-Butadiene (HTPB) II: Implications of the kinetics to combustion of organic polymers. *Combustion and Flame*, 106:131–143.
- [10] Bianchi, D., Nasuti, F., and Martelli, E., 2009. Coupled Analysis of Flow and Surface Ablation in Carbon-Carbon Rocket Nozzles. *Journal of Spacecraft and Rockets*, 46(3):492–500.
- [11] Bianchi, D., Nasuti, F., Onofri, M., and Martelli, E., 2011. Thermochemical Erosion Analysis for Graphite/Carbon-Carbon Rocket Nozzles. *Journal of Propulsion and Power*, 27(1):197–205.
- [12] Bianchi, D., Nasuti, F., Paciorri, R., and Onofri, M., 2011. Hypersonic flow analysis including finite rate ablation thermochemistry. In Proc. 5th European Conference for Aeronautics and Space Sciences (EUCASS), July 1-5, 2011, Munich, Germany.
- [13] Bianchi, D. and Nasuti, F., 2012. Numerical Analysis of Nozzle Material Thermochemical Erosion in Hybrid Rocket Engines. AIAA Paper 2012-3809.
- [14] Milos, F. S., and Rasky, D. J., 1994. Review of Numerical Procedures for Computational Surface Thermochemistry. *Journal of Thermophysics and Heat Transfer*, 8(1).
- [15] Kendall, R. M., Bartlett, E. P., Rindal, R. A., and Moyer, C. B., 1968. An Analysis of the Chemically Reacting Boundary Layer and Charring Ablator. Part I: Summary Report. NASA CR 1060.
- [16] Bianchi, D., Nasuti, F., Martelli, E., and Onofri, M., 2007. A numerical approach for high-temperature flows over ablating surfaces. In Proc. 39th AIAA Thermophysics Conference, June 2007, Miami, FL.
- [17] Chelliah, H. K., Makino, A., Kato, I., Araki, N., and Law, C. K., 1996. Modeling of Graphite Oxidation in a Stagnant-Point Flow Field Using Detailed Homogeneous and Semiglobal Heterogeneous Mechanisms with Comparisons to Experiments. *Combustion and Flame*. 104(4).
- [18] Bradley, D., Dixon-Lewis, G., Habik, S. E., and Mushi, E. M., 1984. The Oxidation of Graphite Powder in Flame Reactions Zones, *Twentieth Symposium (International) on Combustion*. 931–940. The combustion Institute, Pittsburgh.
- [19] Acharya, R. and Kuo, K. K., 2007. Effect of Pressure and Propellant Composition on Graphite Rocket Nozzle Erosion Rate. *Journal of Propulsion and Power*. 23(6):1242–1254.

- [20] Thakre, P. and Yang, V., 2008. Chemical Erosion of Carbon-Carbon/Graphite Nozzles in Solid-Propellant Rocket Motors. *Journal of Propulsion and Power*. 24(4):822–833.
- [21] Nagle, J. and Strickland-Constable, R. F., 1962. Oxidation of Carbon Between 1000-2000 $\hat{\text{A}}^{\circ}\text{C}$ - *Proceedings of the Fifth Carbon Conference*. 1:154–164, Pergamon Press, Inc.
- [22] Geisler, R. L. and Beckman, C. W., The History of the BATES Motors at the Air Force Rocket Propulsion Laboratories, AIAA Paper 98–3981, 1998.
- [23] Gordon, S. and McBride, B. J., Computer Program for Calculation of Complex Chemical Equilibrium Compositions and Applications, NASA RP 1311, 1994.